Investigation of microstructure and tribological property of Ti-6Al-4V alloy by laser shock peening processing

Cheng Gu
Zenghui Tian
Jian hua Zhao (zjhwzf@sina.com)
Chongqing University
Yajun Wang

Research Article

Keywords: Laser shock peening, Microstructure, Tribological property, Ti-6Al-4V alloy

Posted Date: April 3rd, 2023

DOI: https://doi.org/10.21203/rs.3.rs-2738156/v1

Version of Record: A version of this preprint was published at The International Journal of Advanced Manufacturing Technology on September 25th, 2023. See the published version at https://doi.org/10.1007/s00170-023-12354-5.

Abstract

Laser shock peening (LSP) is a process to introduce compressive residual stresses for improved surface properties of materials. In this study, the effect of LSP on the microstructure and tribological property of Ti-6Al-4V alloy was investigated. The surface and cross-sectional microstructure of the samples show that the shape of the β phase changes from a long strip to a short bar and granular after the LSP treatment. With the increase of laser energy, the surface roughness decreases gradually while the surface microhardness is increased. The maximum hardness is on the surface, and with the increase of the depth, the hardness decreases until a stable value of 339.4 HV which is the microhardness of the matrix. The thickness of the high-microhardness layer is about 350 μm. LSP treatment can decrease the average friction coefficient and effectively improve the tribological property of Ti-6Al-4V alloy. The higher the laser energy, the better the wear resistance. This study is helpful for further study and applications of the LSP process in improving the tribological property of Ti alloys.

1. Introduction

As one of the typical α+β dual-phase titanium alloys, Ti-6Al-4V alloy has the advantages of high specific strength, good corrosion resistance, and stable physical and chemical properties, which has been widely used in aerospace, medical and other fields [1-3]. However, the tribological properties and fatigue resistance of Ti-6Al-4V alloy are relatively low, so it is difficult to meet the long-term performance requirements of key components in complex service environments [4-6]. To improve the service life of structural materials, various surface modification technologies without changing the matrix material have been applied to Ti alloys such as mechanical shot peening (SP) [7], surface mechanical attrition treatment (SMAT) [8], deep cold rolling (DCR) [9], laser shock peening (LSP) [10], and so on. Compared with other methods, LSP has the advantages of an outstanding strengthening effect, wide application range, strong controllability, and good applicability [11, 12].

LSP can induce the residual compressive stress of a certain amplitude and depth on the metal surface and refine the surface grain to improve comprehensive properties such as fatigue resistance, corrosion resistance, and wear resistance [13-16]. As the schematic diagram shown in **Fig. 1**, LSP uses a high-frequency, high-power, and short-pulse laser beam to impact the workpiece surface with an absorption layer through the intermediate restraint layer. The absorption layer rapidly evaporates and ionizes under laser irradiation, forming high-temperature and high-pressure plasma, which propagates into the workpiece under the action of the confinement layer. Due to the peak pressure of the shock wave being much higher than the dynamic yield strength of the material, a high strain rate of plastic deformation and residual compressive stress layer with large depth (up to 1-2 mm) and high amplitude (hundreds of MPa) are produced in the material [17-21]. Therefore, applying LSP can change the surface and internal structure of the material and improve the comprehensive properties of the material.

Recently, research has been performed in the field of LSP, mainly focusing on common metal materials such as steel [22], aluminum alloy [23], and titanium alloy [24]. Bai et al. [25] studied the improvement of

the life cycle performance of high-strength steel by LSP from the aspects of microhardness, residual stress, and corrosion resistance. Ding et al. [26] investigated the changes in dislocation density and grain size in the microstructure of LY2 aluminum alloy after LSP by finite element simulation. Lainé et al. [27] found that LSP produced directional planar dislocations and networks of dislocation cells and sub-grains. Jia et al. [28] investigated the changes in the microhardness and residual stress layer of Ti834 alloy after LSP treatment and proposed the microstructure evolution mechanism of Ti834 alloy through microscopic observation. Liao et al. [29] found that the surface grain of the sample was refined and the surface microhardness was increased by 11.6% after LSP. Lin et al. [30] showed that with the increase of laser shock time or energy, the microhardness of Ti-6Al-4V alloy increased significantly. Madapana et al. [31] found that the surface grains of Ti-6Al-4V alloy was refined after LSP treatment, and the surface roughness increased with the increase of laser intensity. Although research on the effect of LSP on Ti-6Al-4V alloy has been performed, there are few studies on the microstructures, surface integrity, and tribological property. It is important to complete the study on the effect of LSP on the tribological property of Ti alloys.

In this article, Ti-6Al-4V alloy was subjected to laser shock treatment with different laser energy. Compared with untreated samples, the effects of LSP on the surface morphology, roughness, microhardness, and tribological property of Ti-6Al-4V alloy were investigated. The wear mechanism of the untreated and LSP-treated samples was discussed.

2. Materials and methods

Ti-6Al-4V alloy was selected as the experimental material with the chemical composition of Ti-6.1Al-3.9V. The as-cast Ti-6Al-4V plates were treated by high-temperature rolling at 920℃ and heat treatment at 750℃ for 1 h and then cooled in the air. After that, the samples were ultrasonically cleaned with acetone and ethanol solution to remove surface stains.

In the LSP experiment, YS100-R200A Nd: YAG laser was used. The schematic diagram of the laser shock path is shown in **Fig. 2**. Different laser energies of 6 J, 7 J, and 8 J were used in the experiment. A black tape with a thickness of 100 μm was used as the energy absorption layer to ensure that the material surface was not burned by a high-energy laser. A uniform water flow layer of approximately 2 mm thickness was used as the confinement layer to increase the peak pressure of the laser shock wave. Other parameters used in the LSP process are shown in **Table 1**.

Table 1 Main parameters used in the LSP process.

Parameters	Pulse duration	Pulse wavelength	Overlapping ratio	Spot diameter
Value	20 ns	1064 nm	50%	3 mm

After the LSP treatment, the samples were cut by electric discharge machining (EDM) to the size of 20 mm × 10 mm × 2 mm. The cross-sections of the samples were polished, etched by Keller etchant, and

cleaned by absolute ethanol.

X-ray diffraction (XRD, AD/max 2500PC) was used to measure the phase composition of the samples with Cukα radiation (λ= 0.1541 nm) scanning at a rate of 4°/min in 2θ degree between 20°-90°. Scanning electron microscope (SEM, TESCAN VEGA 3 LMH) and energy dispersive spectrometer (EDS) were used to analyze the microstructure and composition of the samples. A laser scanning confocal microscope (LSCM, OLS300) was used to characterize the surface morphology, surface roughness, and 3D profile of the samples. The MH-5L Vickers microhardness tester was used to measure the microhardness. The load was 100 g, and the holding time was 10 s. At the same depth, average microhardness was calculated by 10 measured points. The wear test was carried out on the untreated sample and the LSP-treated sample by MDW-2 high-speed wear tester. An Al_2O_3 ball with a diameter of 10 mm was used as the test piece. The contact mode was ball-disc, and the lubrication mode was dry friction. The wear test was carried out at a room temperature of 20 ℃ with a reciprocating stroke of 12 mm, normal load of 5 N, working frequency of 2 Hz, and wear time of 5 minutes.

3. Results And Discussion

3.1. Microstructure

The XRD patterns of the untreated sample and LSP-treated samples are shown in **Fig. 3**. It can be seen that the Ti-6Al-4V sample is composed of the α phase with HCP structure and the β phase with BCC structure. The α phase shows a multi-angle diffraction peak, but the β phase in the (110) direction does not show an obvious diffraction peak. After the LSP process, it is found that the diffraction peak of the α phase is weakened and some diffraction peaks are widened. There is no new phase generated, which indicates that no phase change occurs during the LSP process. This is because the thermal effect of the LSP is lower than the phase transition temperature of the Ti-6Al-4V alloy.

The surface microstructures of the untreated sample and LSP-treated samples are shown in **Fig. 4**. As can be seen in **Fig. 4(a)**, the phase structure distribution on the surface is relatively uniform. After the LSP treatment, the phase structures become larger, which may be due to the transformation and connection between the phase structures. However, according to the EDS element map, there is less difference in the distribution of elements after the LSP treatment.

Fig. 5 shows the cross-sectional microstructures of untreated sample and LSP-treated samples. As can be seen from **Fig. 5(a)**, the light gray α phase shows a large area of a continuous distribution mixed with the bright white strip β phases. The volume fraction of the β phase is small and dispersed throughout the matrix. In the meantime, the distribution of the β phase presents to be directional, which is caused by the hot rolling process. After the LSP process, the β phase is refined which changes from slender strips to short rods and granules as shown in **Fig. 5(b)-(d)**. In **Fig. 5(c)-(d)**, it can be seen that some tissue structures show a wide range of banded connection characteristics. Sun et al. [32] reported that there are

high-density dislocations and stacking faults on the surface layer after LSP, the grains were refined and nano-grains existed.

3.2. Surface roughness

The 3-D morphologies of the untreated and LSP-treated sample surfaces were observed by laser scanning confocal microscope as shown in **Fig. 6**. It can be seen that the surface of the untreated sample is uneven. The surface shows relatively large undulations with some bumps and pits. After the LSP treatment as shown in **Fig. 6(b)-(d)**, the surfaces are relatively flat with convex structures and there are no obvious concave features. It shows that the bumps and pits at the surface are reduced after the LSP process. Moreover, it can be found that with the increase of laser energy, the surface roughness is reduced. The surface roughness of the untreated sample in **Fig. 6(a)** is 0.685 μm which is the largest among the four samples. With the increase of laser energy in the LSP treatment, the surface roughness decreases. The lowest surface roughness is 0.583 μm when the laser energy is 8 J as shown in **Fig. 6(d)**.

Due to the Gaussian distribution of laser energy on the sample surface, uneven plastic deformation occurs on the surface of Ti-6Al-4V alloy. During the LSP process, the interior of the sample is affected by the plasma shock wave, and irreversible plastic deformation will occur when the stress peak exceeds the elastic limit of the material. Along the impact direction, the compression plastic deformation layer with a certain depth will form. The shock wave as well as the material in the compression plastic deformation layer will spread to both sides along the direction perpendicular to the propagation of the shock wave. Both the plastic deformation and the material transfer will help reduce the bumps and pits on the surface of the sample, affecting the surface morphology and roughness.

The 2-D profile curve of the Ti-6Al-4V sample surface was also characterized as shown in **Fig. 7**. It can be seen the surface profile curve of the untreated sample fluctuates greatly, and the height difference is about 7.04 μm. After the LSP process, the height difference of the surface of the sample is lower than that of the untreated sample. The height differences of the LSP-treated samples with laser energy of 7 J and 8 J are 4.84 μm and 5.91 μm, respectively. This phenomenon is slightly different from the variation characteristics of surface roughness. The main reason for the change in surface roughness is the plastic deformation of the surface caused by laser shock. In the LSP process, the material surface undergoes elastic-plastic deformation, in which irreversible plastic deformation makes the metal in the impact zone flow along the surface to the outer edge, forming plastic deformation flow. Under the effect of the laser shock and the surrounding metals, local uneven plastic deformation will be formed in the shock area. These local plastic deformations will affect the distribution of convex and concave features, resulting in the change of surface roughness of the sample. Therefore, the LSP process helps weaken the existence of convex features and reduce surface roughness. The impact with higher laser energy will lead to a decrease in roughness which is different from the research [33] that the surface roughness increases with the increase of laser energy. The reason may be that the roughness measured in this study is in the local region of around 650 μm.

3.3. Microhardness

The microhardness at the surface and along the depth direction of the untreated sample and LSP-treated samples were measured as shown in **Fig. 8.** In the untreated sample, the microhardness along the depth direction shows to be between 338.9 HV and 339.7 HV, and the average value is 339.4 HV. It can be seen that the surface microhardness of Ti-6Al-4V alloy is increased after LSP treatment. The peak microhardness of the LSP-treated samples with the laser energy of 6 J, 7 J, and 8 J are 387.3 HV, 392.4 HV, and 396.1 HV, respectively. After LSP treatment, the microhardness at the surface increased by 14.12%, 15.63%, and 16.70% compared with the untreated sample. With the increase of laser energy, the peak microhardness is increased. This is because the pressure produced by laser shock is as high as several GPa, which leads to plastic deformation with a high strain rate of 10^7 s^{-1} on the surface region of the material, which promotes the nucleation and growth of dislocations and the generation of twins, stacking faults, and other defects. With the increase of laser energy, more energy will be transferred to the Ti-6Al-4V matrix, resulting in more serious plastic deformation. And, the probability of defect formation such as dislocations, twins, and stacking faults will be increased with the increase of laser energy, which will eventually lead to an increase in microhardness.

It also can be seen in **Fig. 8** that, from the surface to the interior of the LSP-treated sample, the microhardness has a decreasing trend until a stable value of 339.4 HV which is the microhardness of the matrix. The decreasing trend of microhardness of samples with different impact energy is the same, and the thickness of the high-microhardness layer is about 350 μm. It is because the shock wave produced by LSP gradually is weakened with the increase of propagation depth. The degree of plastic deformation of the material also gradually decreases, which makes the microhardness of the material gradually decrease and stabilize in the range of matrix hardness. Zhang et al. [34] found that the high density of dislocations promoted the increase of the microhardness of the material surface. Based on the relationship between the microhardness and dislocation density [35], the increase of microhardness after LSP is closely related to the high dislocation density on the surface layer. According to the Hall-Petch relation [36], the strength of a material is inversely proportional to its grain size. In the LSP process, the laser-induced shock wave has intense interaction with the material, which leads to an increase in dislocation density and grain refinement on the surface of the material. As a result, the microhardness and surface strength can be increased after the LSP process.

3.4. Tribological property

The wear test was carried out to investigate the effect of LSP on the tribological property of Ti-6Al-4V alloy. The variation curve of the friction coefficient with time is shown in **Fig. 9**. It can be seen that the changing trends of friction coefficients of all the untreated sample and the LSP-treated samples are almost the same. A similar trend shows to be increasing until stable. At the initial stage, the friction coefficient increases rapidly, which is the running-in stage of the wear process. The initial contact area between the friction pair and the surface of the sample is small and the wear is serious. The irregular

protrusions on the surface are destroyed at the initial stage and fall off to form hard particles on the worn surface. During the wear test, the wear debris on the surface of Ti-6Al-4V gradually increases, which will accumulate on the wear surface to hinder sliding, increasing the friction coefficient. In the meantime, the contact mode between Al_2O_3 grinding ball and the worn surface changes from point-to-surface contact to surface-to-surface contact.

It also can be seen in **Fig. 9** that the friction coefficient of the samples after the LSP treatment is smaller than that of the untreated sample. Moreover, with the increase of laser energy, the average friction coefficient decreases. It shows that the LSP process is beneficial to improve the tribological property of Ti-6Al-4V alloy.

The average friction coefficient is further calculated to directly express the wear resistance as shown in **Fig. 10**. As can be seen that the average friction coefficients of the untreated sample and LSP-treated samples with laser energy of 6 J, 7 J, and 8 J are 0.34, 0.31, 0.29, and 0.24, respectively. The average friction coefficient of untreated samples is the largest, and the average friction coefficient decreases after the LSP treatment. Moreover, with the increase of laser energy, the average friction coefficient of the LSP-treated sample decreases which shows that the wear resistance of the samples has been improved.

It is known that the surface roughness of materials has an important influence on wear performance. The rougher the surface of the material, the greater the friction coefficient produced during the wear process. Moreover, it is easy for the rough surface to produce wear debris at the initial stage, which harms the wear resistance. In this study, the surface roughness of the sample is reduced after the LSP treatment, which is beneficial to the tribological property of the Ti-6Al-4V alloy. The decrease in the average friction coefficient is consistent with the results of the surface roughness. According to Holm-Archard [37], hardness is one of the important indexes to measure the tribological property of materials. The greater the surface hardness of the material, the better the wear resistance of the material. In addition, the thicker the hardness strengthening layer, the longer the fatigue life of the material.

Fig. 11 shows the wear morphology of the untreated sample and LSP-treated samples. To quantitatively analyze the worn surface, 3-D images of the worn surface were observed by using a laser scanning confocal microscope as shown in **Fig. 12**. As shown in **Fig. 11(a)**, on the surface of the untreated sample, there are many fine wear debris, groove friction marks with different depths, and a small number of pitting pits. On the surface of the LSP-treated samples as shown in **Fig. 11(b)-(d)**, the width of the furrow is smaller compared with that of the untreated sample, and there are more plastic deformation layers as shown in **Fig. 12(b)-(d)**. However, there are several large particles on the surfaces of the LSP-treated samples.

EDS point scanning was carried out on the surfaces of the samples and the results are shown in **Table 2**. The results of points 1, 3, and 7 indicate that there is oxygen existed in the large particles. Points 4 and 5 show there is also oxygen existing on the edge of the plastic deformation layer but the content is less.

There is no oxygen observed in the Ti-6Al-4V substance. The large particles do not fall off from the plastic deformation layer and can be oxidized during the wear test.

Table 2 EDS analysis of the wear surface of Ti-6Al-4V samples.

at. %	Ti	Al	V	O
1	33.33	12.83	1.78	52.07
2	83.43	12.24	4.33	
3	23.72	18.82	1.21	56.25
4	56.66	22.48	3.34	17.52
5	67.38	11.21	3.88	17.53
6	84.43	10.81	4.76	
7	41.34	17.2	2.95	38.51
8	83.67	11.45	4.88	

In the wear test under normal load, the sample surface in contact with the Al_2O_3 grinding ball deforms at first, and then falls off, forming a large number of irregular abrasive dust. At this stage, the friction coefficient will increase rapidly. When the surface is rougher, more debris will generate at the initial stage, which is consistent with the trend obtained in **Fig.9**. Since the abrasive dust content increases with time, the hard oxide particles participate in the friction process, promoting the occurrence of abrasive wear. The abrasive particles slide along the surface of the sample during the wear test, which results in furrows and micro-cuttings on the surface as shown in **Fig. 11** and **Fig. 12**. It can be seen that the furrow morphology occupies most of the worn surface, which indicates that abrasive wear plays a leading role in the wear test. On the other hand, the hard oxide abrasive particles and abrasive marks can produce stress concentration on the surface during the wear test, which leads to the nucleation and growth of microcracks. The growth of the cracks will lead to a peeling and pitting phenomenon and eventually cause fatigue wear on the surface. According to the EDS results in **Table 3**, there is oxygen existed in the debris, which indicates that oxidative wear occurs during the wear process. It can be seen that the wear mechanism of the Ti-6Al-4V includes the synergistic effect of abrasive wear, fatigue wear, and oxidation wear.

4. Conclusion

In this article, the effect of LSP on the microstructure, surface roughness, microhardness, and tribological property of the Ti-6Al-4V alloy was investigated. Different laser energies were used in the experiments. The main conclusions are as follows:

(1) During the LSP process of Ti-6Al-4V alloy, the phase composition does not change much. The surface and longitudinal section of the samples show that the shape of the β phase changes from a long strip to a short bar and granular after the LSP treatment.

(2) By applying LSP treatment, the convex structure on the surface and the surface roughness is reduced. With the increase of laser energy from 6 J to 8 J, the surface roughness decreases gradually.

(3) LSP treatment can increase the microhardness on the surface layer of Ti-6Al-4V alloy. The maximum hardness is on the surface, and with the increase of the depth, the hardness decreases until a stable value of 339.4 HV which is the microhardness of the matrix. With the increase of laser energy, the peak microhardness is increased. The decreasing trend of microhardness of samples with different laser energies is the same, and the thickness of the high-microhardness layer is about 350 μm.

(4) LSP treatment can effectively improve the tribological property of Ti-6Al-4V alloy. The higher the laser energy, the better the wear resistance. It is found that the wear mechanism of the Ti-6Al-4V includes the synergistic effect of abrasive wear, fatigue wear, and oxidation wear.

Declarations

CRediT authorship contribution statement

Cheng Gu: Conceptualization, Investigation, Formal analysis, Writing - review & editing. **Zenghui Tian**: Investigation, Formal analysis, Writing - original draft. **Jianhua Zhao**: Investigation, Conceptualization, Formal analysis, Hypothesis, Writing - review & editing. **Yajun Wang**: Investigation.

Data availability

All data that support the findings of this study are available from the corresponding author upon reasonable request.

Competing Interests

The authors declare no competing interests.

Materials availability

Not applicable.

Code availability

Not applicable.

Funding

The authors would like to acknowledge the financial supports from the National Natural Science Foundation of China (NO. 51875062 and NO. 52205336), and the China Postdoctoral Science Foundation (No. 2021M700567).

References

1. Zhang J, Cheng X, Xia Q ,Yan C (2020) Strengthening effect of laser shock peening on 7075-T6 aviation aluminum alloy. Adv. Mech. Eng. 12.http://10.1177/1687814020952177
2. Fu Y, Wu Q, Yang W ,Liu S (2022) Synthesis and Properties of Hydrogels on Medical Titanium Alloy Surface by Modified Dopamine Adhesion. Gels 8.http://10.3390/gels8080458
3. Gao H, Shi X, Xue Y, Zhang K, Huang Q, Wu C, Ma J ,Shu J (2022) Tribological Behaviors and Friction-Induced Vibration and Noise Performance of TC4 with Microporous Channels Filled by Sn-Ag-Cu and Nb2C. J. Mater. Eng. Perform.http://10.1007/s11665-022-07189-2
4. Su B, Wang H, Cao Y, Pei X ,Hua G (2020) Local deformation and macro distortion of TC4 titanium alloy during laser shock processing. The International Journal of Advanced Manufacturing Technology 106:5421-5428.http://10.1007/s00170-020-05058-7
5. Zhao Z, Wang L, Zhang J, Liu L ,Chen W (2021) Prediction of high-cycle fatigue strength in a Ti-17 alloy blade after foreign object damage. Eng. Fract. Mech. 241.http://10.1016/j.engfracmech.2020.107385
6. Zhao J, Shangguan J, Gao L, Gu C, Wang Y ,Shi Y (2022) New Insights into Microstructure Characteristics and Tribological Property of Ti Alloy Processed by Hot-Dip Aluminizing and Heat Treatment. Metallurgical and Materials Transactions A 53:1035-1050.http://10.1007/s11661-021-06575-0
7. Wang L, Zhou L, Liu L, He W, Pan X, Nie X ,Luo S (2022) Fatigue strength improvement in Ti-6Al-4V subjected to foreign object damage by combined treatment of laser shock peening and shot peening. Int. J. Fatigue 155.http://10.1016/j.ijfatigue.2021.106581
8. Chen A, Wang C, Jiang J, Ruan H ,Lu J (2021) Microstructure Evolution and Mechanical Properties of Austenite Stainless Steel with Gradient Twinned Structure by Surface Mechanical Attrition Treatment. Nanomaterials (Basel) 11.http://10.3390/nano11061624
9. Nagarajan B, Kumar D, Fan Z ,Castagne S (2018) Effect of deep cold rolling on mechanical properties and microstructure of nickel-based superalloys. Materials Science and Engineering: A 728:196-207.http://10.1016/j.msea.2018.05.005
10. Gu H, Yan P, Jiao L, Chen S, Song Y, Zou S ,Wang X (2023) Effect of laser shock peening on boring hole surface integrity and conformal contact fretting fatigue life of Ti-6Al-4 V alloy. Int. J. Fatigue 166.http://10.1016/j.ijfatigue.2022.107241
11. Liao Y, Ye C ,Cheng G J (2016) [INVITED] A review: Warm laser shock peening and related laser processing technique. Opt. Laser Technol. 78:15-24.http://10.1016/j.optlastec.2015.09.014

12. Nie X, He W, Cao Z, Song J, Li X, Pang Z ,Yan X (2021) Experimental study and fatigue life prediction on high cycle fatigue performance of laser-peened TC4 titanium alloy. Materials Science and Engineering: A 822.http://10.1016/j.msea.2021.141658
13. Maharjan N, Chan S Y, Ramesh T, Nai P G ,Ardi D T (2020) Fatigue performance of laser shock peened Ti6Al4V and Al6061-T6 alloys. Fatigue & Fracture of Engineering Materials & Structures 44:733-747.http://10.1111/ffe.13390
14. Park J, Yeo I, Jang I ,Jeong S (2019) Improvement of friction characteristics of cast aluminum-silicon alloy by laser shock peening. J. Mater. Process. Technol. 266:283-291.http://10.1016/j.jmatprotec.2018.11.007
15. Sanchez A G, Leering M, Glaser D, Furfari D, Fitzpatrick M E, Wharton J A ,Reed P a S (2021) Effects of ablative and non-ablative laser shock peening on AA7075-T651 corrosion and fatigue performance. Mater. Sci. Technol. 37:1015-1034.http://10.1080/02670836.2021.1972272
16. Sun R, Li L, Guo W, Peng P, Zhai T, Che Z, Li B, Guo C ,Zhu Y (2018) Laser shock peening induced fatigue crack retardation in Ti-17 titanium alloy. Materials Science and Engineering: A 737:94-104.http://10.1016/j.msea.2018.09.016
17. Lim H, Kim P, Jeong H ,Jeong S (2012) Enhancement of abrasion and corrosion resistance of duplex stainless steel by laser shock peening. J. Mater. Process. Technol. 212:1347-1354.http://10.1016/j.jmatprotec.2012.01.023
18. Wang C, Wang L, Wang C-L, Li K ,Wang X-G (2020) Dislocation density-based study of grain refinement induced by laser shock peening. Opt. Laser Technol. 121.http://10.1016/j.optlastec.2019.105827
19. Zhao M, Duan C, Li J ,Luo X (2019) Deformation and Residual Stress Characteristics of TC17 Alloy Subjected to Laser Shock Peening with Single and Double Sides. IOP Conf. Ser.: Mater. Sci. Eng. 493.http://10.1088/1757-899x/493/1/012001
20. Kalainathan S ,Prabhakaran S (2016) Recent development and future perspectives of low energy laser shock peening. Opt. Laser Technol. 81:137-144.http://10.1016/j.optlastec.2016.02.007
21. Montross C S, Wei T, Ye L, Clark G ,Mai Y W (2002) Laser shock processing and its effects on microstructure and properties of metal alloys: a review. Int. J. Fatigue 24:1021-1036.http://10.1016/s0142-1123(02)00022-1
22. Chen H, Wei C, Wang S, Jiang Z, Peng X, Cao Z ,Shao J (2021) Effects of laser shock peening on the properties and microstructure evolution of laser-polished surface of Cr12 steel. J. Laser Appl. 33.http://10.2351/7.0000395
23. Meng X-K, Wang H, Tan W-S, Cai J, Zhou J-Z ,Liu L (2020) Gradient microstructure and vibration fatigue properties of 2024-T351 aluminium alloy treated by laser shock peening. Surf. Coat. Technol. 391.http://10.1016/j.surfcoat.2020.125698
24. Li J, Zhou J, Liu L, Feng A, Huang S ,Meng X (2021) High-cycle bending fatigue behavior of TC6 titanium alloy subjected to laser shock peening assisted by cryogenic temperature. Surf. Coat. Technol. 409.http://10.1016/j.surfcoat.2021.126848

25. Bai Y, Wang H, Wang S, Huang Y, Chen Y, Zhang W, Ostendorf A ,Zhou X (2021) Life cycle strengthening of high-strength steels by nanosecond laser shock. Appl. Surf. Sci. 569.http://10.1016/j.apsusc.2021.151118
26. Ding H, Li Y, Zhang Z ,Yuan D (2019) Analysis of microstructural evolution properties based on laser shock peening. Optik 179:361-366.http://10.1016/j.ijleo.2018.10.165
27. Lainé S J, Knowles K M, Doorbar P J, Cutts R D ,Rugg D (2017) Microstructural characterisation of metallic shot peened and laser shock peened Ti–6Al–4V. Acta Materialia 123:350-361.http://10.1016/j.actamat.2016.10.044
28. Jia W, Zan Y, Mao C, Li S, Zhou W, Li Q, Zhang S ,Ji V (2021) Microstructure evolution and mechanical properties of a lamellar near-α titanium alloy treated by laser shock peening. Vacuum 184.http://10.1016/j.vacuum.2020.109906
29. Liao L, Gao R, Yang Z H, Wu S T ,Wan Q (2022) A study on the wear and corrosion resistance of high-entropy alloy treated with laser shock peening and PVD coating. Surf. Coat. Technol. 437.http://10.1016/j.surfcoat.2022.128281
30. Lin Y, Ding S Y, Zhou L C, He W F, Cai Z B, Wang W J ,Zhou Z R (2019) Influence of laser shock peening parameters on the abrasive wear behavior of TC4 titanium alloy under controlled cycling impact. Materials Research Express 6.http://ARTN 09654610.1088/2053-1591/ab2e60
31. Madapana D, Ramadas H, Nath A K ,Dutta Majumdar J (2022) Studies on Laser Shock Peening on Nanomechanical and Mechano-Chemical Properties of Titanium Alloy (Ti6Al4V). JOM.http://10.1007/s11837-022-05504-9
32. Sun R, Cao Z, Zhang Y, Zhang H, Yu Y, Che Z, Wu J, Zou S ,Guo W (2021) Laser Shock Peening of SiCp/2009Al Composites: Microstructural Evolution, Residual Stress and Fatigue Behavior. Materials (Basel) 14.http://10.3390/ma14051082
33. Chukwuike V I, Echem O G, Prabhakaran S, Anandkumar S ,Barik R C (2021) Laser shock peening (LSP): Electrochemical and hydrodynamic investigation of corrosion protection pre-treatment for a copper surface in 3.5 % NaCl medium. Corros. Sci. 179.http://10.1016/j.corsci.2020.109156
34. Zhang X C, Zhang Y K, Lu J Z, Xuan F Z, Wang Z D ,Tu S T (2010) Improvement of fatigue life of Ti–6Al–4V alloy by laser shock peening. Materials Science and Engineering: A 527:3411-3415.http://10.1016/j.msea.2010.01.076
35. Nix W D ,Gao H J (1998) Indentation size effects in crystalline materials: A law for strain gradient plasticity. J. Mech. Phys. Solids 46:411-425.http://10.1016/s0022-5096(97)00086-0
36. Stjohn C F ,Teghtsoo.E (1965) GRAIN SIZE DEPENDENCE OF FRACTURE IN ALPHA-URANIUM. J. Nucl. Mater. 17:111-&.http://10.1016/0022-3115(65)90027-9
37. Corrochano J, Walker J C, Lieblich M, Ibáñez J ,Rainforth W M (2011) Dry sliding wear behaviour of powder metallurgy Al–Mg–Si alloy-MoSi2 composites and the relationship with the microstructure. Wear 270:658-665.http://10.1016/j.wear.2011.01.029

Figures

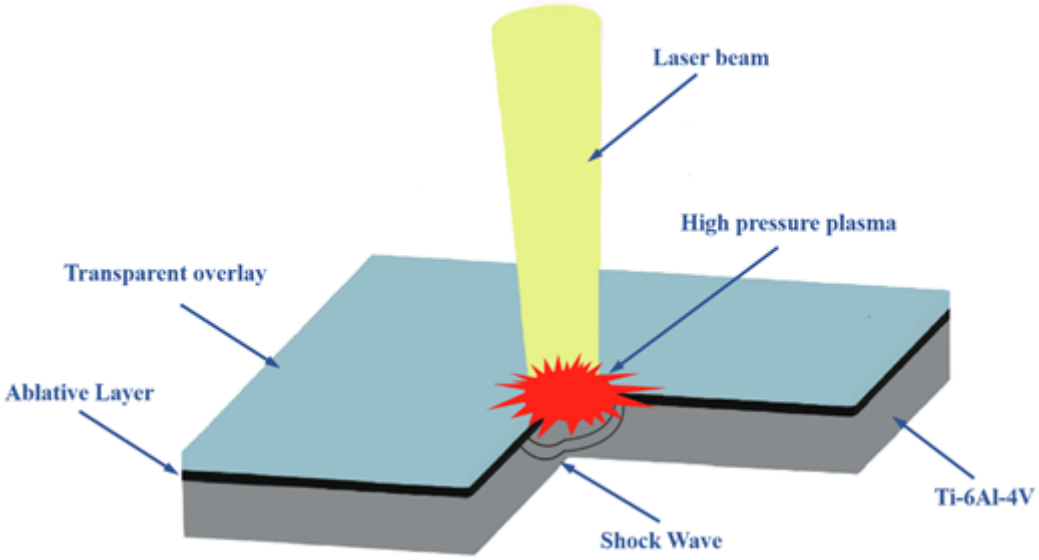

Figure 1

Schematic diagram of LSP principle.

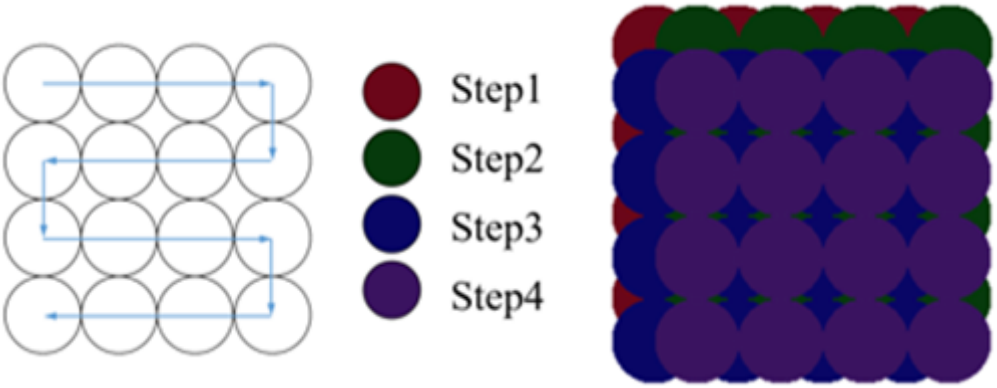

Figure 2

Schematic diagram of the scanning path of the LSP process.

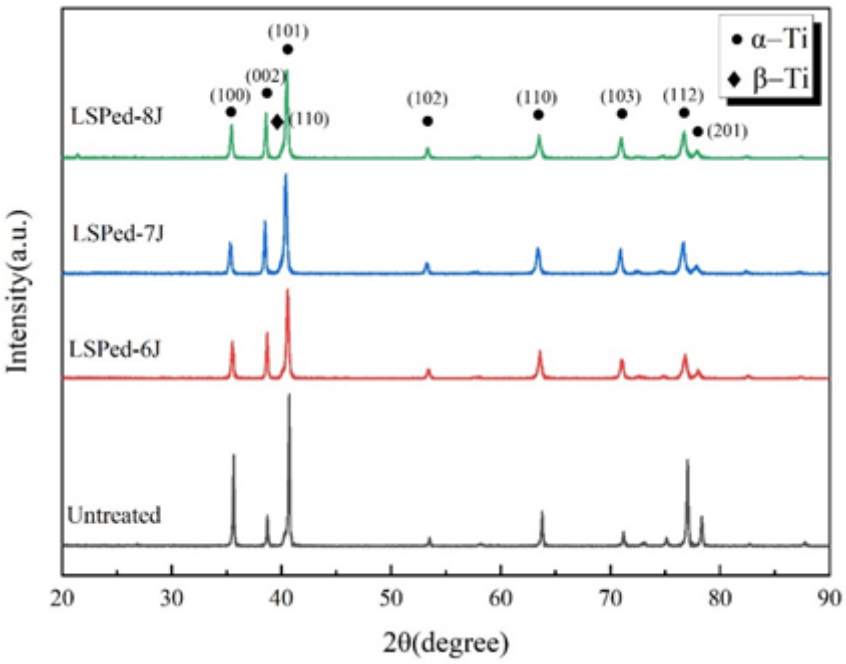

Figure 3

XRD patterns of the untreated and LSP-treated Ti-6Al-4V samples.

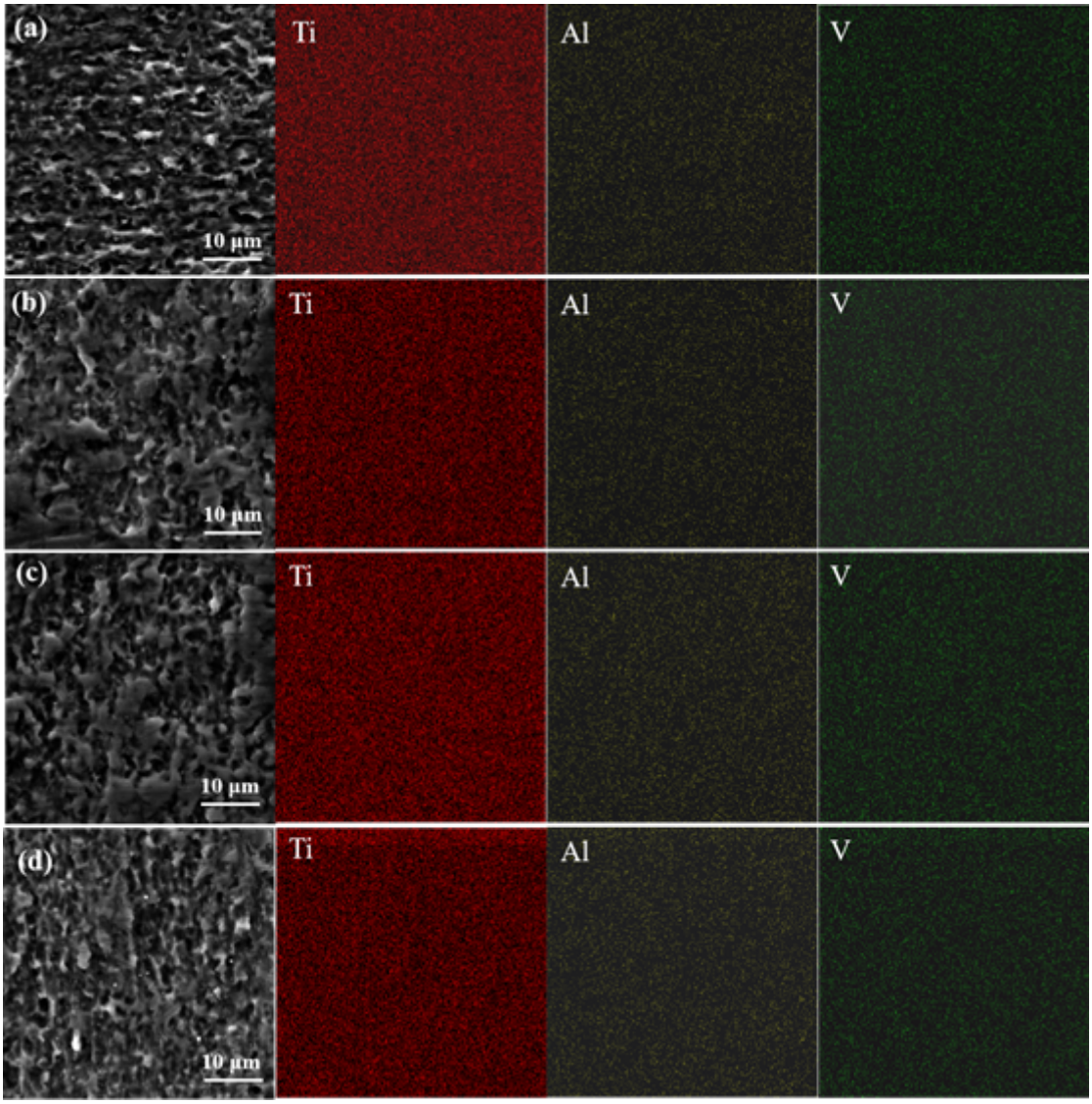

Figure 4

Surface microstructures of (a) the untreated Ti-6Al-4V sample, and the LSP-treated samples with laser energy of (b) 6 J, (c) 7 J, and (d) 8 J.

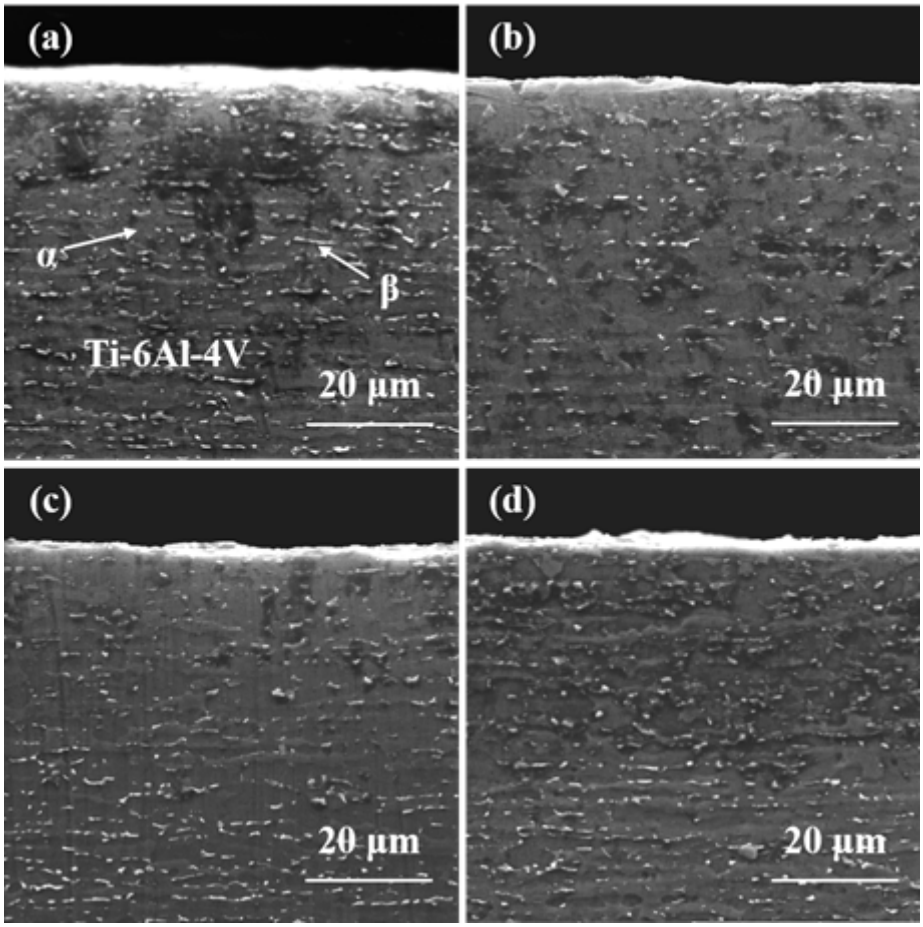

Figure 5

Cross-sectional microstructures of (a) the untreated Ti-6Al-4V sample, and the LSP-treated samples with laser energy of (b) 6 J, (c) 7 J, and (d) 8 J.

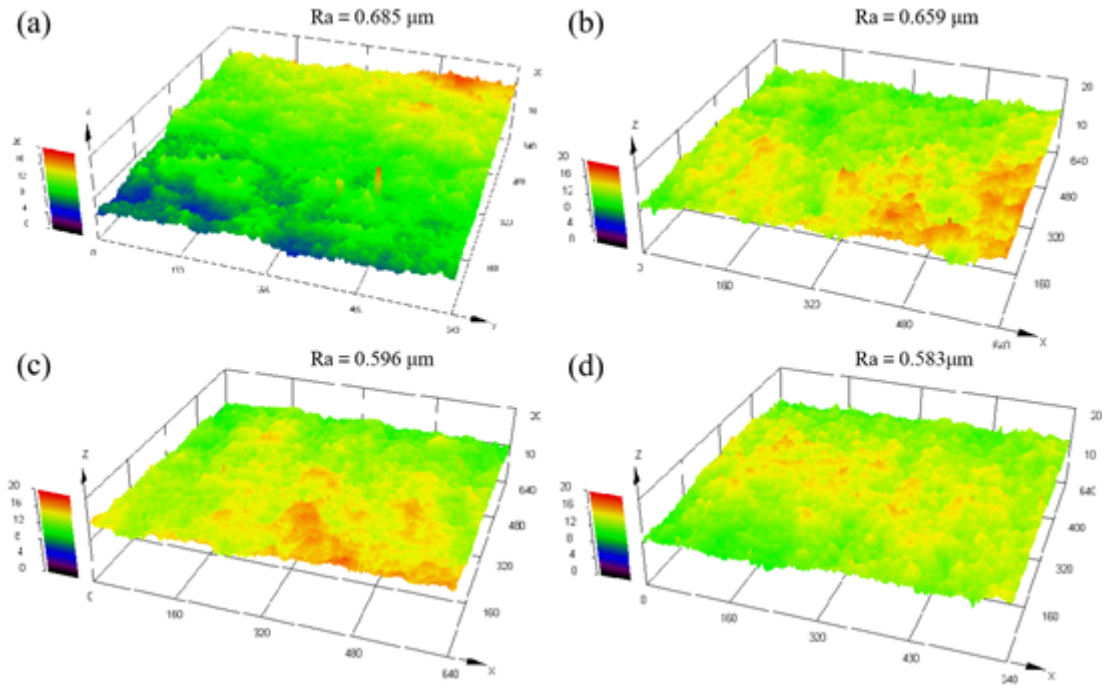

Figure 6

3-D morphology and surface roughness of (a) the untreated Ti-6Al-4V sample, and the LSP-treated samples with laser energy of (b) 6 J, (c) 7 J, and (d) 8 J.

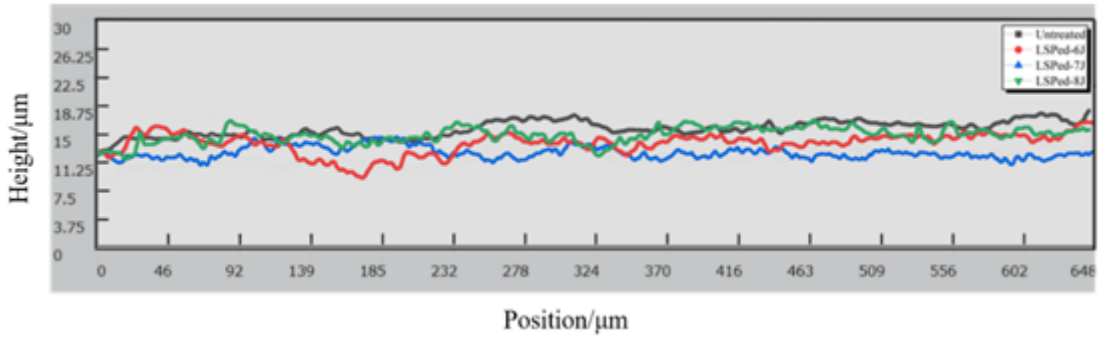

Figure 7

2-D contour curves of the surface of the untreated and the LSP-treated Ti-6Al-4V samples.

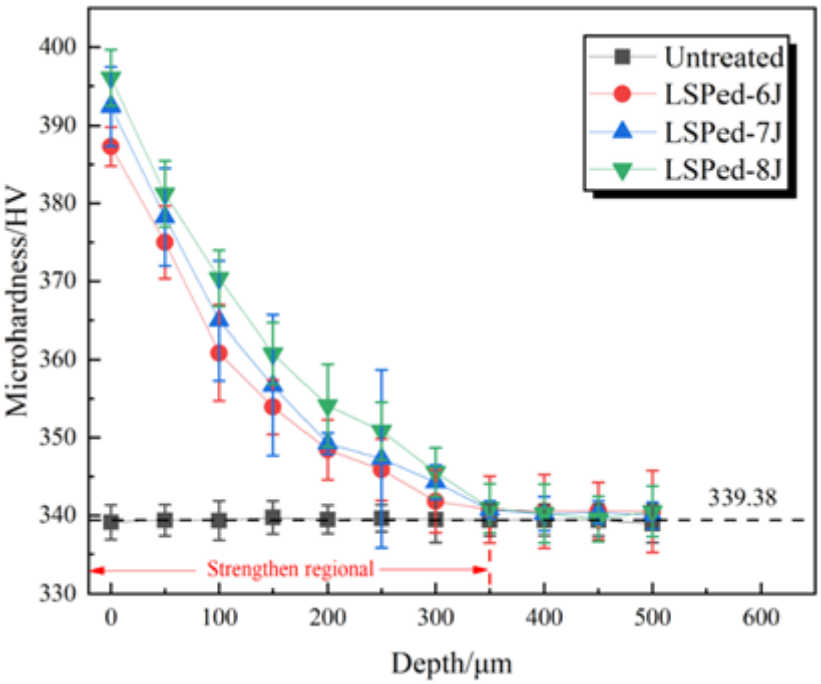

Figure 8

Microhardness profiles of the untreated and the LSP-treated Ti-6Al-4V samples along the depth direction.

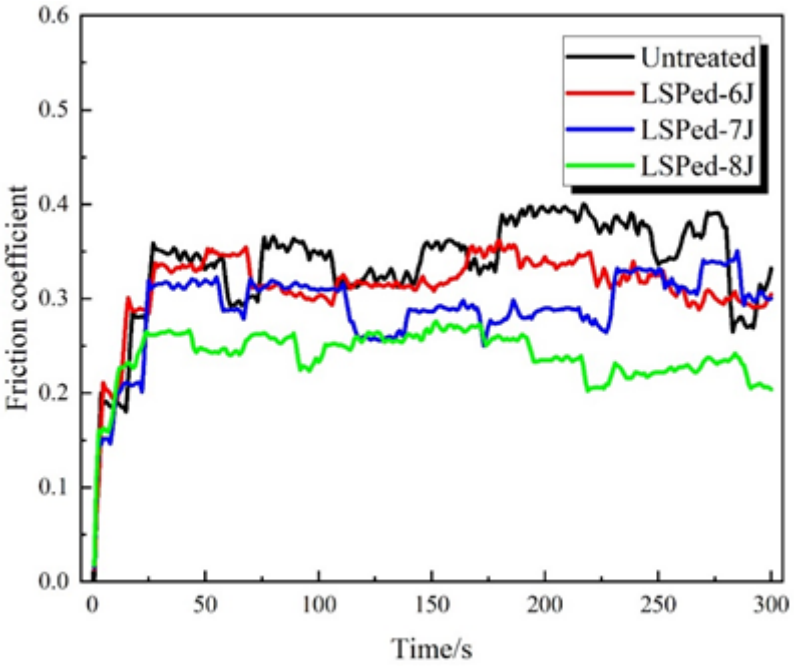

Figure 9

Friction coefficient of the untreated and the LSP-treated Ti-6Al-4V samples as a function of time.

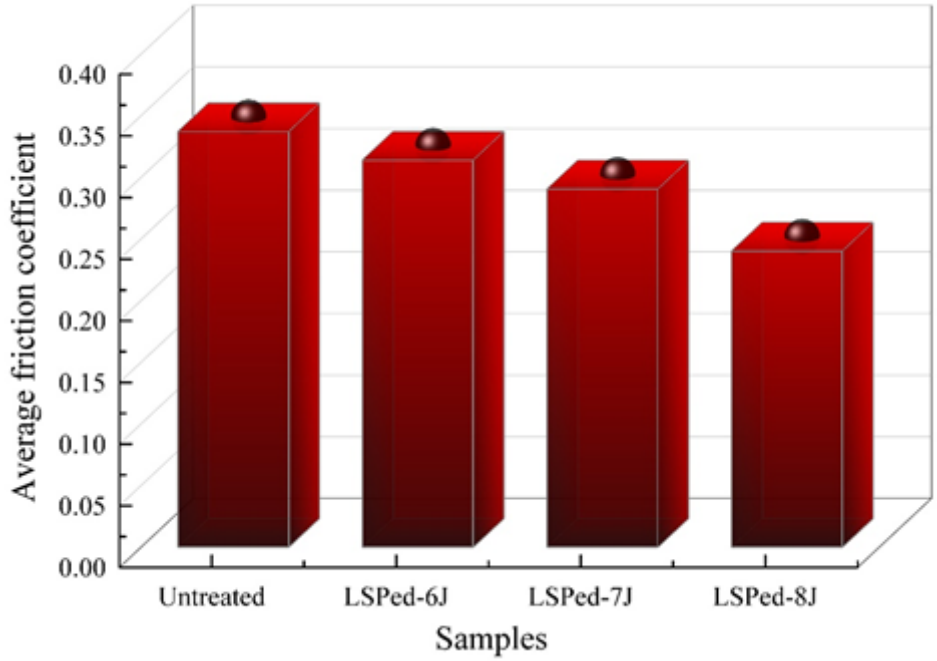

Figure 10

Average friction coefficient of the untreated and the LSP-treated Ti-6Al-4V samples.

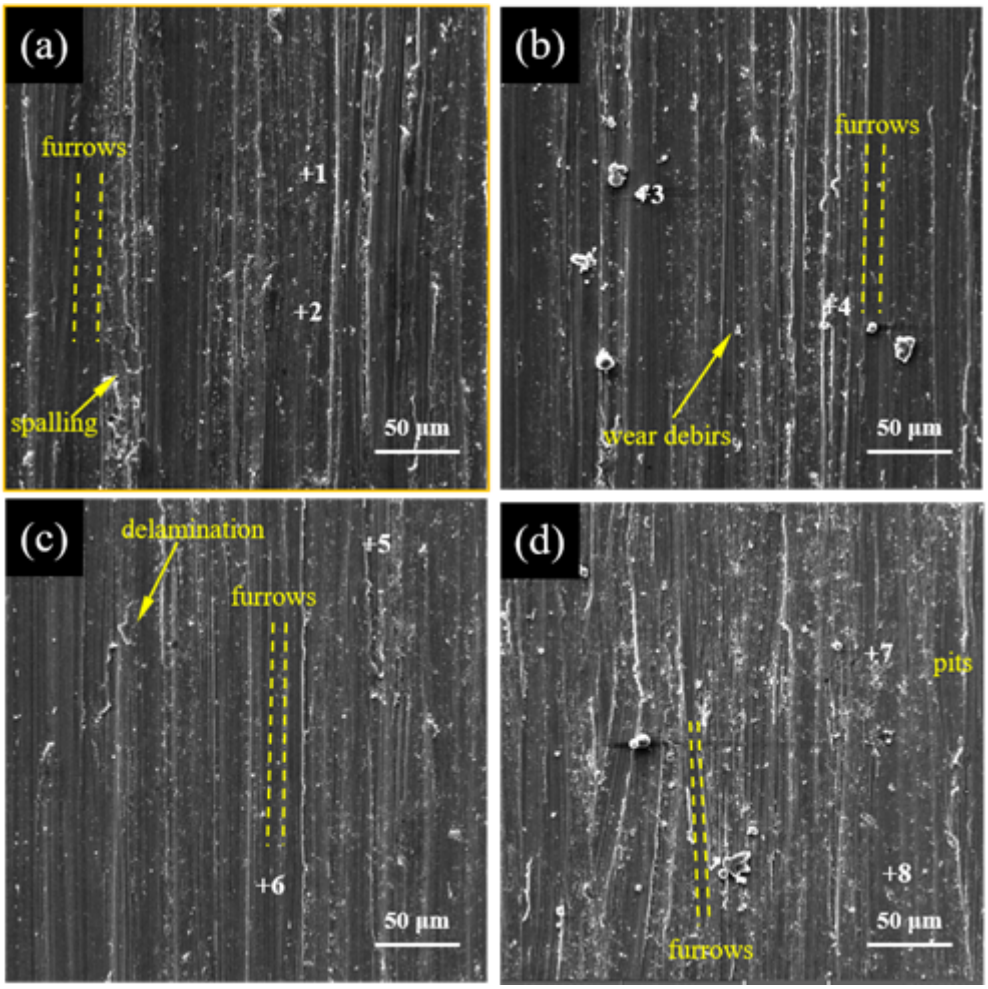

Figure 11

Microstructure of the wear surface of (a) the untreated Ti-6Al-4V sample, and the LSP-treated samples with laser energy of (b) 6 J, (c) 7 J, and (d) 8 J.

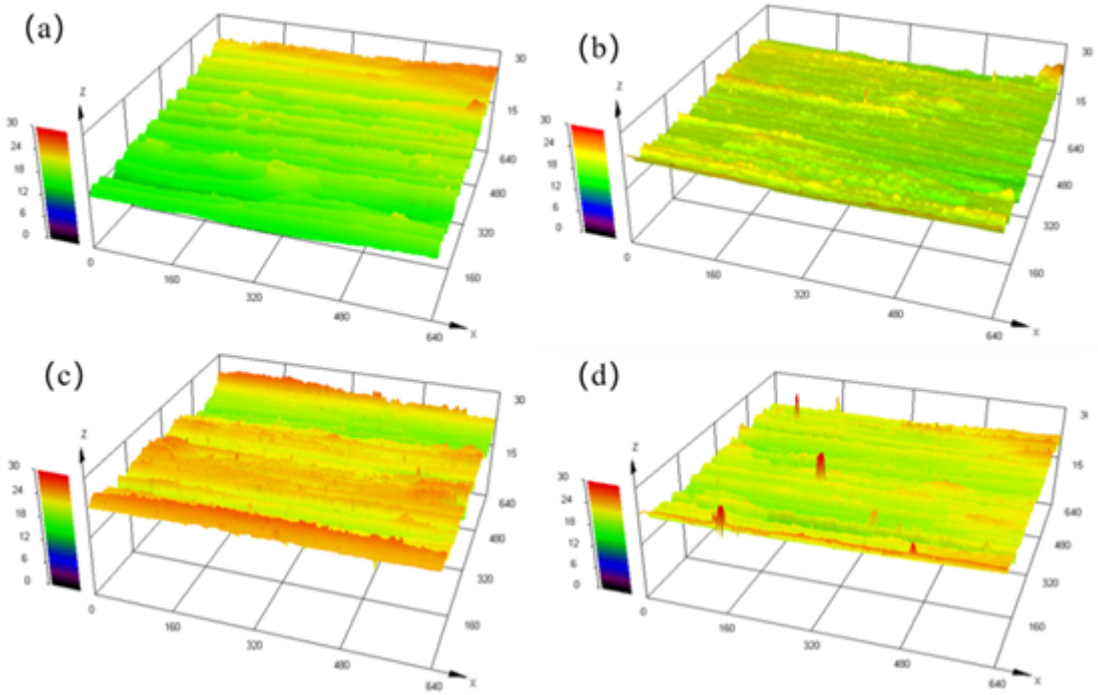

Figure 12

3-D image of the worn surface of (a) the untreated Ti-6Al-4V sample, and the LSP-treated samples with laser energy of (b) 6 J, (c) 7 J, and (d) 8 J.